Chapter 4

Sedimentation velocity analytical ultracentrifugation

Stephen E. Harding

NCMH Physical Biochemistry Laboratory, University of Nottingham, School of Biosciences, Sutton Bonington, Leicestershire LE12 5RD, UK.

Donald J. Winzor

Centre for Protein Structure, Function and Engineering, Department of Biochemistry, University of Queensland, Brisbane, Queensland 4072, Australia.

1 Introduction: sedimentation velocity and sedimentation equilibrium

There has been a general misconception amongst biochemists that the analytical ultracentrifuge does not provide an absolute means of molecular mass determination and hence of the characterization of interaction phenomena. This has arisen from a lack of awareness about the difference between the two types of experiment that can be performed in the analytical ultracentrifuge.

(a) **Sedimentation velocity**: an experiment performed at sufficiently high speed for the centrifugation of solute away from the centre of rotation to be monitored as the rate of movement of a sedimenting boundary. For a given rotor speed, solvent viscosity and solvent density the rate of migration depends upon the overall size and shape of the macromolecule or macromolecule-ligand complex.

(b) **Sedimentation equilibrium**: an experiment performed at a lower speed so that the sedimentation and back-diffusion forces are of comparable magnitudes and therefore give rise to an equilibrium distribution of solute concentration. Because there is no net transport at equilibrium, shape effects do not come into play and the distribution becomes an absolute function of molecular mass for a single solute. For an interacting system the distribution is an absolute reflection of the mass action relationship between the species participating in the chemical equilibrium reaction (concentrations as well as molecular masses of the participating species).

The criticism that analytical ultracentrifugation does not provide an absolute determination of molecular mass thus only applies to sedimentation velocity,

which can nevertheless be used to great effect in the identification and characterization of solute–ligand interactions. In such studies one needs to allow for the effects of shape on the sedimentation coefficients of putative solute–ligand complexes—allowances that become less equivocal for the interaction of a protein with a small ligand ($M < 500$). Indeed, sedimentation velocity studies have been crucial to detection of the conformational changes associated with the allosteric regulation of aspartate transcarbamylase (1) and pyruvate kinase (2). On the grounds that biochemists tend to be more familiar with the technique of sedimentation velocity, this variant of analytical ultracentrifugation for the study of acceptor–ligand systems is addressed in the current chapter: the following chapter considers the application of sedimentation equilibrium for the same purpose. Although treated separately, a combination of the two types of ultracentrifuge measurement can often provide an even greater inroad into the understanding of interactions between macromolecular acceptors and a wide range of ligand types.

2 Basic principles of sedimentation velocity

Before the user embarks on the analysis of interacting systems—which can present a number of difficulties—he/she needs to have a grasp for the basic principles of sedimentation velocity: we start by outlining the original (and still used) procedure for determining the sedimentation coefficient of a non-interacting solute, which for the purposes of illustration is taken to be a homogeneous protein.

2.1 Measurement of a sedimentation coefficient

A solution of protein is placed in a specially designed cell in which the sector-shape of the channels in the centrepiece (*Figure 1*) allows unimpeded migration of protein molecules in a radially outward direction in response to the applied centrifugal field. One sector is filled with protein solution and the other with buffer to provide a reference cell for the absorption and Rayleigh optical systems. At the commencement of a sedimentation velocity experiment the concentration of solute is uniform throughout the cell, but subjection of the solution column to a high centrifugal field (typically 50 000–60 000 r.p.m. for a protein with a molecular mass of 10–100 kDa) leads to progressive removal of solute from the inner region of the cell (*Figure 2*). Migration of the moving boundary of solute is recorded optically, and the sedimentation coefficient, s_A, then determined from its definition (rate of migration per unit field), namely:

$$s_A = (dr_p/dt)/(\omega^2 r) = (d \ln r_p/dt)/\omega^2 \qquad [1]$$

where r_p denotes the radial position of the protein boundary after centrifugation for time t at angular velocity ω, which is expressed in radians per second (1 revolution $= 2\pi$ radians, and $\omega =$ r.p.m. $\times 2\pi/60$). The linear dependence of

(a)   (b)   (c)
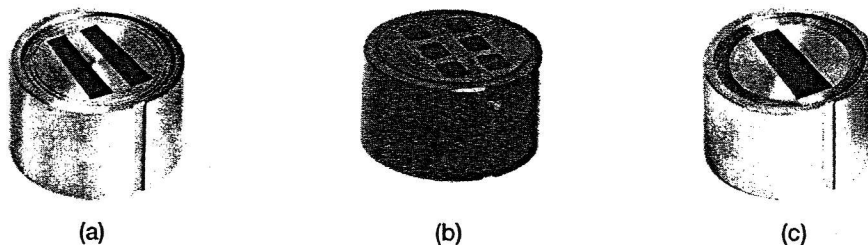
Figure 1 Centrepieces commonly used in an ultracentrifuge cell (Photograph courtesy of Beckman Instruments, Palo Alto, USA). (a) Standard 12 mm optical path length double sector. Used in XL-A, XL-I, and Model E ultracentrifuges. A range of centrepiece materials are available: users should check the inertness of the solvent in their solutions. One sector used for solution, the other for reference solvent. (b) Six channel (12 mm). Three solution/solvent pairs. These are generally used only for sedimentation equilbrium measurements because (i) the shorter solution column length requirements; (ii) a speed limitation of ∼ 40 000 r.p.m. (c) Single channel (12 mm). For the Model E ultracentrifuge only, and not suitable for sedimentation equilibrium experiments. Users should familiarize themselves with the difference between 'optical path length' and 'solution column length'. Standard cell centrepieces are 12 mm optical path length for the XL centrifuges. Shorter path lengths are available to attenuate optical signals (e.g. lower the UV absorbance). Long (30 mm) path length cells for amplification of optical signals can be used in Model E but not in XL ultracentrifuges. Solution column lengths are typically 10 mm for sedimentation velocity (corresponding to ∼ 0.4 ml in a 12 mm path length cell) and ∼ 3 mm for sedimentation equilibrium (corresponding to ∼ 0.1 ml).

ln r_p upon t thus has a slope of $\omega^2 s_A$. The sedimentation coefficient has units of time, which are usually reported in Svedberg units S (1 S = 10^{-13} sec).

For a spherical solute with molecular mass M_A and a radius a the value of the sedimentation coefficient measured at temperature T in buffer b, $(s_A)_{T,b}$, is related to molecular parameters by the expression:

$$(s_A)_{T,b} = M_A(1 - \bar{v}_A \rho_{T,b})/(N 6 \pi \eta_{T,b} a) \qquad [2]$$

where N is Avogadro's number and $\bar{v}_A$ is the partial specific volume of the protein (effectively the reciprocal of the solute density): the other two parameters refer to the density ($\rho_{T,b}$) and viscosity ($\eta_{T,b}$) of the buffer medium in which the solute is migrating. For a non-spherical solute the same expression is used except that a now refers to the radius of the equivalent hydrodynamic sphere—the source of the dependence of sedimentation coefficient upon shape of the solute. To take into account the dependence of $(s_A)_{T,b}$ upon solvent parameters, sedimentation coefficients are corrected to values for migration in a solvent with the density and viscosity of water. From *Equation 2* the corrected value, $(s_A)_{20,w}$, is therefore:

$$(s_A)_{20,w} = (s_A)_{T,b}(\eta_{T,b}/\eta_{20,w})[(1 - \bar{v}_A \rho_{20,w})/(1 - \bar{v}_A \rho_{T,b})] \qquad [3]$$

where $\eta_{20,w}$ and $\rho_{20,w}$ are the viscosity and density respectively of water at 20 °C.

Because its derivation is based on the premise of unhindered migration, *Equation 2* refers to the sedimentation coefficient of solute in infinitely dilute solution, $(s_A^{\circ})_{20,w}$—a parameter that needs to be obtained from the dependence
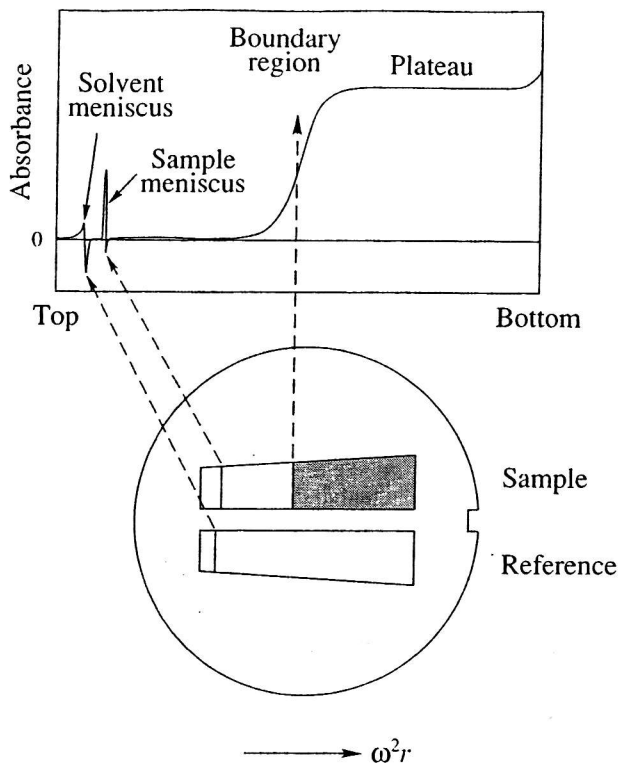
Figure 2 Plan view of a double sector centrifuge cell during a sedimentation velocity experiment and corresponding UV absorption optical record. The sample solution is placed in one sector and a sample of the solvent in the reference sector. The reference sector is usually filled slightly more than the sample sector, so that the reference meniscus does not obscure the sample profile. For simplicity the boundary in the schematic cell is shown as infinitely sharp: because of diffusion effects this will not be the case, as reflected in the scan. From ref. 80, and reproduced courtesy of Beckman Instruments. (NB. For sedimentation equilibrium experiments (Chapter 5), the reference channel should contain solvent that has been in dialysis equilibrium with the sample solution.)

of $(s_A)_{20,w}$ upon the weight-concentration of solute, c_A. For proteins this dependence is of the form:

$$(s_A)_{20,w} = (s_A^{\circ})_{20,w}(1 - k_s c_A) \qquad [4]$$

where the Gralén coefficient k_s is in the vicinity of 0.007 ml/g. For nucleic acids and polysaccharides the concentration dependence is expressed more appropriately in the form:

$$(s_A)_{20,w} = (s_A^{\circ})_{20,w}/(1 + k_s c_A + ...) \qquad [5]$$

2.2 Measurement of molecular mass by sedimentation velocity

Unequivocal determination of M_A from sedimentation velocity experiments requires replacement of the $(6\pi\eta_{T,b}a)$ term in *Equation 2* by an independent

measure of the frictional coefficient, $f_A = 6\pi\eta_{T,b}a$: the diffusion coefficient, $(D_A)_{T,b}$, provides such a means. Combination of the description of the diffusion coefficient in molecular terms:

$$(D_A)_{T,b} = RT/(Nf_A) = RT/(6\pi\eta_{T,b}a) \qquad [6]$$

where R is the universal gas constant, with Equation 2 gives rise to the Svedberg equation,

$$M_A = RT(s_A)_{T,b}/[(D_A)_{T,b}(1 - \bar{v}_A\rho_{T,b})] \qquad [7]$$

The diffusion coefficient can be measured independently in a separate experiment; but advantage is frequently taken of the Lamm equation for centrifugal migration:

$$r(dc_A/dt) = -d[s_A\omega^2 rc_A - D_A(dc_A/dr)]/dr \qquad [8]$$

to obtain estimates of the diffusion coefficient from the extent of boundary spreading in a sedimentation velocity experiment. Any such value is, of course, an apparent diffusion coefficient because its elucidation is based on the premise that diffusion is the sole cause of boundary spreading, i.e. on the premise that the solute is homogeneous.

The lack of an analytical solution to this differential equation prompted the use of approximate solutions, the most notable of which is that obtained by Fujita (3) for the situation in which s_A varies linearly with solute concentration but D_A is constant (4–7). Currently, however, the requirement of an analytical solution to Equation 8 is being obviated by employing numerical integration—a procedure which has the potential to allow the incorporation of concentration dependence of the diffusion coefficient as well as the sedimentation coefficient (8–14).

Protocol 1

Sedimentation velocity: basic operation and measurement of a sedimentation coefficient

Equipment and reagents

- Ultracentrifuge
- Optical system
- Protein
- Buffer

Method

1 Concentration requirements of the protein. This depends on the interaction being investigated. If it is a self-association and interaction strengths are being probed, the initial cell-loading concentrations chosen should be such that there are measurable amounts of reactants and products present.

2 Optical system: this depends on the concentration range and the protein. For absorption optics a minimum cell loading concentration equivalent to 0.1 absorbance units is required. An absorbance of 1.4 is the likely upper limit for strict adherence with the Lambert–Beer proportionality between absorbance and concentration—a limit

Protocol 1 continued

that is more critical in sedimentation equilibrium than in sedimentation velocity studies. For solutions with absorbance values greater than 3 shorter path length cells need to be employed (the minimum is about 3 mm). Although the absorbance can be decreased by a change to a less sensitive wavelength, the preferred alternative is a switch to interference or schlieren optics. Conventional cells (pathlength 12 mm) are usable down to about 0.1 mg/ml and up to 5 mg/ml if shorter cells are used. Above 5 mg/ml, schlieren optics are the only real option: consult an advanced user.

3   Choose the appropriate buffer/solvent. If possible, work with an aqueous solvent of sufficiently high ionic strength (> 0.05 M) to provide adequate suppression of non-ideality phenomena deriving from macromolecular charge effects. If denaturing/dissociating solvents are used, appropriate centrepieces need to be used (e.g. of the Kel-F type from Beckman instruments).

4   Load the sample into the cell. Double sector cells are used with the protein solution or protein–ligand solution (0.2–0.4 ml) in one sector and the reference buffer or solvent in the other. The latter is filled to a slightly higher level to avoid complications caused by the signal coming from the solvent meniscus; the scanning system subtracts the absorbance of the reference buffer from that of the sample. Electronic multiplexing allows multiple hole rotors to be used, so that several samples can be run at a time (see text above).

5   Choose the appropriate temperature. The modern XL ultracentrifuges can measure comfortably between 4 °C and 40 °C. For higher temperatures one of the authors (S. E. H.) has a specially adapted Model E ultracentrifuge which will measure up to 85 °C.

6   Choose the appropriate rotor speed. For a small globular protein of sedimentation coefficient ~ 2 Svedbergs (S, where $1S = 10^{-13}$ sec), a rotor speed of 50 000 r.p.m. gives rise to a measurable set of optical records after some hours. For larger protein systems (e.g. 12S seed proteins, 30S ribosomes) speeds below 30 000 r.p.m. can be employed.

7   Measure the sedimentation coefficient, s of the sedimenting component(s) (denoted s_A for the protein 'acceptor'). The sedimenting coefficient is defined by the rate of movement of the (protein) boundary (radial position r_p) per unit centrifugal field (Equation 1). Commercial software is available for identifying the centre of the sedimenting boundary (strictly the '2nd moment' of the boundary is more appropriate; practically there is no real difference). Personal choices vary, but the following options are available.

(a) *Simple boundary analysis*: Plot out the boundaries from the $c(r)$ vs r plots from the absorbance or interference optical records (recorded at appropriate time intervals) using a high resolution printer or plotter and graphically draw a line through the user-identified boundary centres. Then use a graphics digitizing tablet to recapture the central boundary positions as a function of radial position. Routines such as *XLA-PLOT* (15) work out dr_p/dt and hence s, and also a correction of the loading concentration for average radial dilution during the run (caused by the sector shape of the cell channels).

Protocol 1 continued

(b) *Analysis of the entire concentration distribution {c(r) vs r} and its change with time.*

The on-line capture of data from the centrifuge into the computer now makes this type of analysis feasible. There are several routines currently available: popular ones include *SVEDBERG* (16) based on the Lamm (17) equation and *DCDT* (or the more recent version, *'DCDT+'*) (18) based on Rinde's concept of a sedimentation concentration distribution. For monodisperse systems, besides providing an accurate measure of *s*, these routines provide also an estimate for the translational diffusion coefficient, D_A. For polydisperse systems, a weighted-average sedimentation coefficient is returned for each boundary or component resolved. With *DCDT* a genuine distribution of sedimentation coefficient g(s) is *not* returned directly, (i) because of the complication of diffusion: rather it is an 'effective' distribution, $g^*(s)$. However, extrapolation to infinite time using a procedure developed by Van Holde and Weichet (9) and incorporated by B. Demeler into the algorithm *ULTRASCAN* provides a way around this problem; (ii) The 's' itself is an apparent sedimentation coefficient, affected by non-ideality {sometimes this is denoted by 's^*'—so the true notation is $g^*(s^*)$, i.e an 'apparent' distribution of 'apparent' sedimentation coefficients', although most workers quote it as either $g^*(s)$ or $g(s^*)$.}

8 For each protein concentration used, correct s_A to standard conditions using *Equation 3* (and a similar equation for D_A if measured by *Equation 6*): $(D_A)_{20,w} = D_A(\eta/\eta_{20,w})(293/T)$, where T is the temperature at which D_A was measured. In *Equation 3* knowledge of $\bar{v}_A$, a parameter known as the partial specific volume (essentially the reciprocal of the anhydrous macromolecular density), is needed. This parameter can usually be obtained for proteins from amino acid composition data; for most proteins v_A is in the range 0.73–0.74 ml/g. Programmes such as *SEDNTERP* (20) perform this operation, and from provided amino acid (and carbohydrate) composition data estimates $\bar{v}_A$, as well as ε_{278} and the 'hydration' δ (see Section 4). For glycoproteins the carbohydrate composition also has to be considered ($\bar{v}_A \approx 0.6$ ml/g for carbohydrate); and a similar situation pertains to proteins containing prosthetic groups, which also affect the magnitude of $\bar{v}_A$. Where there is doubt, the partial specific volume should be measured experimentally by precision densimetry (21).

9 For a reversible interaction of the type:

$$\text{protein} + \text{ligand} \longleftrightarrow (\text{protein–ligand}) \tag{9}$$
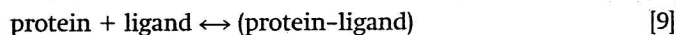
the concentration of protein (and ligand) affects the position of the equilibrium, and hence separate experiments with different loading concentrations are necessary to take into account the effect of concentration upon the sedimentation coefficient. This is discussed in detail later in this chapter. A complication is non-ideality (deriving from the exclusion volume and charge of the macromolecule and/or complex), which is also considered later. The non-ideality is incorporated into the 'Gralén' parameter, k_s, which is related to $s_{20,w}$ and c for dilute solutions of a non-interacting system by *Equations 4* and *5*: this also applies to protein–ligand interacting systems where there is no change in the extent of ligand binding over the concentration range considered.

3 General experimental aspects

Historically, many biochemists have shirked away from ultracentrifuge measurements because of the impression that analytical ultracentrifuges were large bulky instruments which were difficult to operate (correctly) and which yielded photographic records which were tedious to interpret. Such impressions have now changed with the appearance since 1990 of instruments about half of the size of the old traditional ones and with automatic or semi-automatic data capture of the optical records produced via photomultipliers or diode-array camera into a computer. Nonetheless, even with the new generation instruments, for measurements other than simple molecular weight or sedimentation coefficient determination, the general user is still advised to consult the design and interpretation of his/her data with an advanced user since there are many pitfalls awaiting the unwary. Additionally it is worth stressing that there are certain applications where consultation with the advanced user is mandatory. Examples include measurements at high solute concentration that require schlieren (i.e. refractive index gradient optics) or those measurements at low concentration requiring a long optical path length cell. Both types of measurement can only be performed on older instruments still in active use: these remaining few have generally themselves been upgraded with automatic data capture systems.

It is worth stressing that ultracentrifuges generally allow *multiplexing*: that is the analysis of two or more solutions *almost* (i.e. after allowance for the finite time for each scan) simultaneously. This is made possible by multi-hole rotors (four or eight hole with the Beckman XL-A and XL-I instruments, allowing three or seven ultracentrifuge cells respectively—the remaining hole being taken up by the reference counterbalance cell). In addition, special multichannel cells are available which permit more than one solution to be analysed, but these have a rotation speed limit of approximately 40 000 r.p.m. and give data of lower accuracy. *Full advantage should be taken of this opportunity for analysis, under identical experimental conditions, of protein–ligand systems compared against the appropriate controls.*

3.1 Optical systems for sedimentation velocity and sedimentation equilibrium

There are three types of optical detection of centrifuge records (22, 23).

(a) **UV/visible absorbance optics**. The aromatic amino acids tryptophan (Trp) and tyrosine (Tyr) both absorb radiation strongly in the near UV with a maximum at a wavelength of 278 nm. The extinction coefficient, ε_λ, at wavelength λ will depend on the proportion of Trp and Tyr in the amino acid composition: serine will also add slightly to the extinction at 278 nm, and phenylalanine will give a protein some absorbance at 256 nm. The far-UV (190–230 nm) can also be used (where the peptide bond absorbs) *so long as the solvent buffer does not also absorb appreciably*. Detection of the concentration $c(r)$ in terms of absorbance $A_\lambda(r)$ of light of wavelength λ (cm) at a radial position

r (cm) in a centrifuge cell of optical path length l (cm) is based on the Lambert–Beer law:

$$c(r) = A_\lambda(r)/\varepsilon_\lambda l \qquad [10]$$

The two techniques of sedimentation velocity and sedimentation equilibrium have different restrictions with regard to maximum absorbance (considered below).

(b) **Rayleigh interference (refractive index) optics.** All macromolecular solutions have a refractive index, n, greater than that of water (n_o), i.e. they have a positive refraction increment, $n_c = n - n_o$, to an extent which depends on the concentration, c (g/ml) of the macromolecule and the nature of the macromolecule itself, as manifested by the specific refractive increment, dn/dc (ml/g). dn/dc is a parameter in some ways analogous to the extinction coefficient, although unlike ε_{278} it is not heavily dependent on aromatic amino acid content. For proteins $dn/dc \approx 0.19$ ml/g, for carbohydrates it is approximately 0.15 ml/g. It can be measured accurately by refractometry (the accuracy being limited by the accuracy in concentration measurement) or by use of extensive tabulations (24). For a given radial position r in the ultracentrifuge cell $c(r) = n_c(r)/(dn/dc)$. $n_c(r)$ is registered by interference optics with monochromatic (normally laser) light in terms of absolute fringe numbers $J(r) = n_c(r)l/\lambda$: we thus end up with an equation for interference optics analogous to the Lambert–Beer expression, namely:

$$c(r) = J(r)\lambda/[(dn/dc)l] \qquad [11]$$

In practice what is actually measured is the absolute fringe number $J(r)$ relative to the absolute fringe number at the meniscus $J(r_a)$. This relative fringe number, termed $j(r)$, equals $J(r) - J(r_a)$. To obtain $J(r)$ therefore, an estimate of $J(r_a)$ is required. For sedimentation velocity this is normally trivial because $J(r_a) = 0$ after the boundary leaves the meniscus; but for sedimentation equilibrium it is generally not (a matter for the following chapter).

(c) **Schlieren optics.** This optical system records the refractive index (refraction increment) gradient as a function of radial position r:

$$dc(r)/dr = \{1/(dn/dc)\}.dn_c(r)/dr \qquad [12]$$

The choice of optical system depends on whether or not the protein has sufficient absorbing chromophore, the concentration range selected, and the type of experiment (sedimentation velocity or sedimentation equilibrium).

3.2 Sedimentation velocity optical records

Figure 3 shows the type of optical record for monodispersed non-interacting systems from the three types of optical system. The simplest record to visualize and interpret is the UV/visible absorption system (*Figure 3a*) which gives a direct record of concentration $c(r)$ as a function of radial position r, with the concentration expressed in absorbance units, $A_\lambda(r)$, and within the constraints of

(a)

(b)

(c)
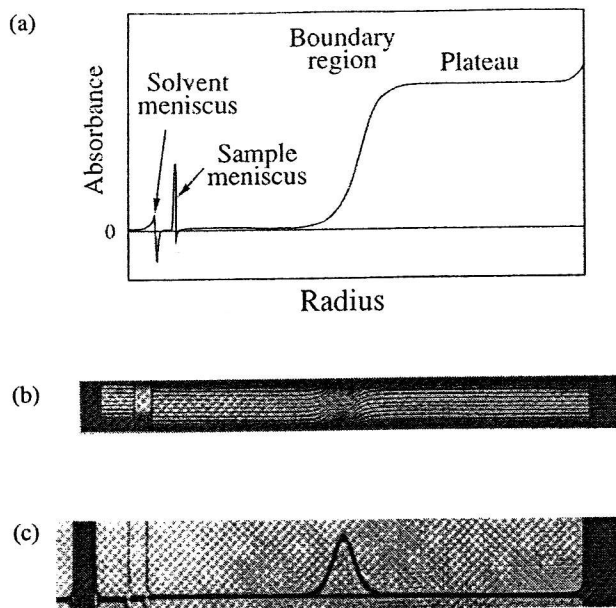
Figure 3 Optical records for sedimentation velocity on homogeneously sedimenting systems. (a) UV absorption (scanned). (b) Rayleigh interference. (c) Schlieren. The optical record in (a) is reprinted from ref. 80, courtesy of Beckman Instruments. (b) and (c) are reprinted from ref. 22, courtesy of Academic Press.

the Lambert–Beer law $\{A_\lambda(r) \propto c(r)\}$. In the interference system (*Figure 3b*) each fringe is a record of concentration $c(r)$ relative to the meniscus, expressed as relative fringe number displacement $j(r)$. The multiple fringes are effectively averaged by a Fourier transform (done automatically by the software coming with the Beckman XL-I) to produce an accurate record of the radial dependence of $j(r)$. On the other hand the schlieren optical record (*Figure 3c*) is a plot of refractive index gradient, $dn_c(r)/dr$, versus radial distance r. Since $n_c(r)$ is proportional to $c(r)$, a concentration gradient is accurately produced. It is possible by integration to produce a plot of $c(r)$ versus r, although for many applications, particularly those involving liganded systems, it is an advantage to have a direct record of the concentration gradient distribution.

3.3 Data capture

There are several options available, as explained in *Protocol 1*. Visual inspection of the $c(r)$ vs r records (absorption/ interference optics) or $dc(r)/dr$ (schlieren optics) vs r can give a rapid idea of the heterogeneity of the system (*Figure 4a,b*) from the number and shape of the boundaries. However, the components need to have quite different sedimentation coefficients; and casual inspection cannot distinguish between a non-interacting mixture of species (a heterogeneous system) and a mixture of species undergoing chemical re-equilibration (a chemically interacting system). Such analysis can be enhanced by transforming

the $c(r)$ vs r plots via the *DCDT* routine (18) into a plot of the apparent distribution of sedimentation coefficient, $g^*(s)$ versus s (see *Protocol 1*) which takes on the appearance of a schlieren diagram (*Figure 4c*) even though the functions describing them are different. The plot of $g^*(s)$ vs s can also be produced from schlieren records (25).

By model-fitting Gaussian distributions to either the $dc(r)/dr$ vs r or $g^*(s)$ vs s diagrams using standard computer packages such as *PRO-FIT* (26), the user can:

(a) Resolve sedimenting components present.

(b) Provide an accurate estimate for the sedimentation coefficient(s) s.

(c) Estimate the amount of each component present.

An important requirement is a minimum number of scans: the helpfiles accompanying the above computer routines should help

3.4 Two complications

There is a complication known as the Johnston–Ogston effect (27) that arises in the analysis of simple mixtures. Because of the inverse dependence of sedimentation coefficient upon solute concentration, the boundary of slower solute is migrating faster than slow solute in the mixture. This leads to a pile-up of slower solute in the region immediately behind the faster-migrating boundary, and hence to overestimation of the proportion of slower-migrating solute: the proportion of faster-migrating solute is correspondingly underestimated.

Another complication is that for a rapid self-association or interaction between solutes of similar size, only a single symmetric boundary may be evident: the sedimentation coefficient obtained in this case is a weighted average of the reactants and product.

3.5 Co-sedimentation diagrams

A useful way of assaying for interactions (other than self-associations) is possible if the reacting species exhibit optical absorption at different regions of the UV/visible spectrum. Optical records of solute distribution are taken at wavelengths where successively one of the reacting species is visible but the other(s) is/are transparent, after which these records are compared with controls of the reactants by themselves at the same concentration (absorbance). This method is particularly useful for monitoring the interaction of a small ligand with a protein. *Figure 5a* illustrates the situation where interaction of the ligand (cofactor B12) with acceptor (methylmalonyl mutase) is stoichiometric (i.e. complete), whereas *Figure 5b* presents a situation involving reversible equilibrium between ligand (methyl orange) and acceptor (bovine serum albumin).

3.6 Concentration dependence of the sedimentation coefficient

For reversible interactions involving protein the concentration of protein and ligand is important. In order to probe the reversible interaction in terms of
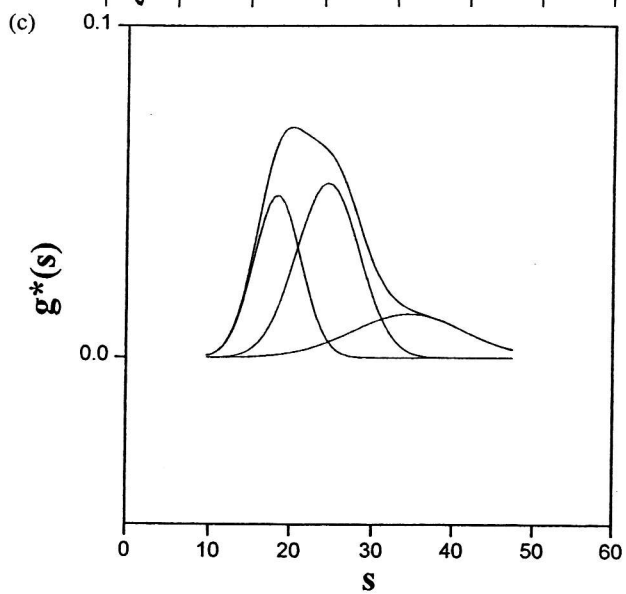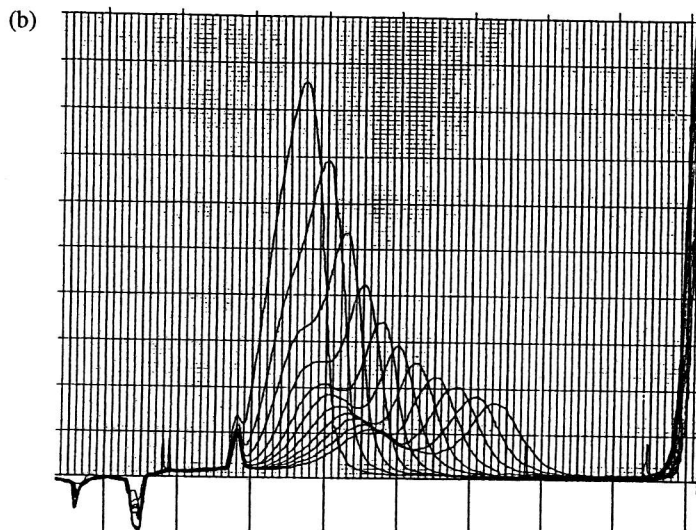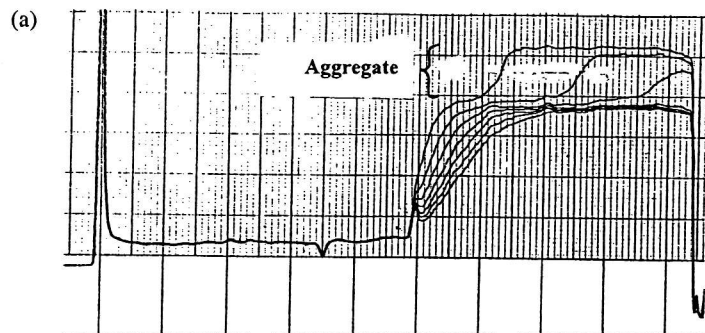
Figure 4 Optical records for mixed solute systems. (a) Scanning UV absorption optical records of the Gene5 protein with aggregate. 0.7 mg/ml, monochromator wavelength 278 nm; scan interval 8 min; rotor speed 40 000 rev/min; temperature 20.0 °C; measured $s_{20,w}$ = (35.3 ± 1.4)S (faster boundary) and (2.6 ± 0.1)S (slower boundary). (From ref. 81.) (b) Scanning schlieren optical records for rat IgE solution with a low molecular weight impurity. 4.52 mg/ml, monochromator wavelength 546 nm; scan interval 8 min; rotor speed 40 000 rev/min; temperature 20.0 °C; measured $s_{20,w}$ = (7.53 ± 0.15) S (IgE) and (3.8 ± 0.1)S (slower impurity). (Davis, K. G., Burton, D. R., and Harding, S. E., unpublished data.) (c) $g*(s)$ vs s (Svedbergs) plots for a trp-mutant GroEL chaperonin system. Upper profile the direct transform from the Rayleigh interference optical record. Lower three profiles from a three component Gaussian fit to these data. Peak maxima, areas respectively are: 1st peak (18.3S, 0.352 units); 2nd peak (24.4S, 0.503 units); 3rd peak (34.5S, 0.229 units). 0.7 mg/ml, number of scans 18; rotor speed 40 000 rev/min; temperature 20.0 °C. Relative peak areas do not change with differing loading concentration, implying the three observed components are NOT in reversible interaction equilibrium. (Walters, C., Clarke, A., and Harding, S. E. unpublished data.)

stoichiometry and strength it is necessary to make measurements over a range of different loading concentrations, since the position of the equilibrium will depend on the concentration of protein (and ligand): higher concentrations will favour the equilibrium towards the right-hand side of *Equation 9*.

(a)

(b)

| 32 min | 48 min | 72 min |
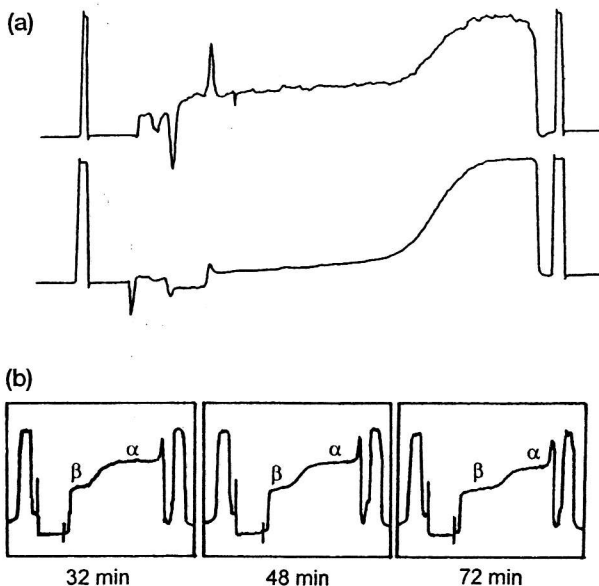
Figure 5 Co-sedimentation diagrams. (a) Absorbance scan for methylmalonyl mutase (0.7 mg/ml) and its cofactor (offset toward the top) scanned within 2 min of each other. The centre of the sedimenting boundary is virtually the same for both, and there is no significant residual absorbance left behind the boundary, suggesting that under the solvent conditions used (50 mM Tris–HCl pH 7.5 + 5mM EDTA) the cofactor ligand is bound to the protein. From ref. 82. Monochromator = 295 nm (bottom), 608 nm (top), rotor speed 44 000 r.p.m. and 20 °C. (b) Absorbance scan for the ligand constituent obtained in a sedimentation velocity experiment after centrifuging a mixture of methyl orange (490 μM) and bovine serum albumin (30 μM) for 32 min at 59 780 r.p.m. and 4 °C. Data are taken from ref. 41.

The appropriate concentration range for study depends on the strength of the interaction, which is either described by the molar association constant K or by the corresponding dissociation constant K_d. For a simple 1:1 stoichiometry, i.e. of the type $A + B \longleftrightarrow AB$, the association constant K_{AB} is related to the molar concentrations C_i of participating species by the expression:

$$K_{AB} = C_{AB}/(C_A C_B) \tag{13}$$

where K_{AB} has units of reciprocal molarity (M^{-1}). For reactions with higher stoichiometry, e.g. $A + 2B \longleftrightarrow AB_2$, the stoichiometric association constant for complex formation from reactants needs to be written as:

$$K_{AB_2} = C_{AB_2}/[C_A C_B{}^2] \tag{14}$$

where the units of K_{AB2} are M^{-2}. Dissociation constants are just the reciprocals of these association equilibrium constants. For 1:1 stoichiometries K_d values below 1 μM tend to be classified as strong interactions, whereas those with $K_d > 50$ μM are often designated as weak interactions.

A complication encountered in the analysis of sedimentation velocity patterns is the non-ideality that derives from the exclusion volume and charge properties of the macromolecule and/or complex. This non-ideality, which is incorporated into the 'Gralén' parameter k_s, is described at low concentration by *Equation 4* for non-interacting globular proteins systems and by *Equation 5* for asymmetric solutes. For higher concentrations additional coefficients can be used in the expansion, as indicated in *Equations 4* and *5*. Alternatively, the concentration dependence may still be written in the form:

$$s^o{}_{20,w} = s_{20,w}(1 - gc) \tag{15}$$

in which g now becomes the following function of c (28):

$$g(c) = \{k_s - [(cv_s)^2(2\phi_p - 1)]/\phi_p{}^2\}/\{k_s c - 2cv_s + 1\} \tag{16}$$

and where v_s is the swollen specific volume (approx. 1 ml/g for globular proteins), ϕ_p a parameter known as the maximum packing fraction by volume, and k_s continues to be the limiting Gralén coefficient (in the absence of associative/dissociative phenomena).

The extraction of K_{AB} (or K_d), by means of the SA-PLOT routine is considered for the ideal and non-ideal cases in Section 5.2.

3.7 Sedimentation coefficient ratios

Another useful criterion for the extent of an interaction involving proteins with other biomolecular species is the ratio of the sedimentation coefficients of the product(s) to the reactant(s). This is particularly useful for the analysis of interactions where large irreversible complexes are formed (29). Provided that assumptions are made about the conformation(s) of reactant(s) and product(s), an estimate for the size/stoichiometry of the complex can be made on the basis of a 'Mark–Houwink–Kuhn–Sakurada' relation (30):

$$(s_{20,w})_{oligomer}/(s_{20,w})_{monomer} = (M_{oligomer}/M_{monomer})^b \tag{17}$$

Similar relations exist for the intrinsic viscosity, translational diffusion coefficient, and radius of gyration. The magnitude of the b coefficient in *Equation 17* depends upon molecular shape: values are ~ 0.67 for spheres, ~ 0.15 for rods, and ~ 0.4–0.5 for coils. In practice the sphere value of 0.67 is usually assumed for globular proteins, together with the further assumption that the conformation of oligomer and monomer are essentially similar. These unsubstantiated assumptions mean that sedimentation velocity studies alone cannot provide unequivocal estimates of interaction stoichiometries, which therefore require confirmation by procedures such as sedimentation equilibrium.

3.8 Sedimentation velocity fingerprinting

For very large protein–biomolecular complexes the sedimentation rates are too fast for measurement even at the lowest practical operating speeds of an analytical ultracentrifuge (1000 rev/min): in such cases reaction products do not remain in solution. A technique known as sedimentation velocity fingerprinting can be used whereby the depletion of reactant concentrations is used to assess the concentration of complex(es) removed from the solution by centrifugation (31).

4 Sedimentation velocity analysis of the shape of a molecular complex

Once the sedimentation coefficient, $s^o_{20,w}$, of the product (and/or the reactants) has been established, the gross conformation or 'shape' of the reaction product can then be examined (29, 32–34), so long as the molecular mass, M, of the product is known, for example, from sedimentation equilibrium. Knowledge of $s^o_{20,w}$ and M permits the evaluation of the translational frictional ratio f/f_o, the ratio of the translational frictional coefficient of the particle to that for a spherical particle of the same mass and anhydrous volume, from the relationship:

$$f/f_o = M_A(1 - \bar{v}_A\rho_{20,w})/[N6\pi\eta_{20,w}s^o_{20,w}\{3M_A\bar{v}_A/4\pi N\}^{1/3}] \qquad [18]$$

where N is Avogadro's number, $\bar{v}_A$ is the partial specific volume of the solute particle. This translational frictional ratio reflects the shape (represented by the parameter P) and state of hydration (δ) of the particle in accordance with the expression:

$$f/f_o = P(1 + \delta/\bar{v}_A\rho_{20,w})^{1/3} \qquad [19]$$

From a practical viewpoint the hydration parameter δ (sometimes denoted as w) is a very difficult parameter to measure with any precision, but can be *estimated* from the amino acid and carbohydrate content (see *Protocol 1*). Values between 0.25 and 0.5 are popularly quoted for this parameter for proteins. From *Equation 19* the shape parameter P, known either as the Perrin parameter or the frictional ratio due to shape, can be evaluated from the experimentally determined f/f_o and a selected value of δ. In practice, a range of plausible values of δ is chosen. Alternatively, δ can be eliminated by combination of f/f_o with other

hydrodynamic measurements such as the intrinsic viscosity, $[\eta]$. The Gralén coefficient k_s, (35) and the ratio $k_s/[\eta]$ are also highly useful in this regard (36).

P is utilized in one of two ways:

(a) Direct evaluation of molecular shape.

(b) Selecting a plausible structure which best agrees with the data.

Some workers relate $s^o_{20,w}$ and $D^o_{20,w}$ directly with shape: we find this route can lead to confusion, especially in regard to the roles of volume and hydration: obtaining shape via the Perrin factor P is recommended.

4.1 Direct evaluation of molecular shape

The axial ratio (a/b)—the ratio of the long to small axis—of the equivalent ellipsoid of revolution (prolate or oblate) can be evaluated using the routine *ELLIPS1* (32). *ELLIPS1* also allows the evaluation of a/b from the complete range of other hydrodynamic measurements. An ellipsoid of revolution has the constraint of two equal axes: a prolate ellipsoid has two equal shorter axes and one longer axis, whereas an oblate ellipsoid has two equal long axes and one shorter axis. A survey of crystal structures has shown the prolate case to be the more appropriate although the distinction can be arbitrary. An alternative representation removes the requirement for two equal axes, but such action requires a more complicated approach using combination of shape functions. An easier alternative is to predict the P (and hence f/f_o, $s^o_{20,w}$) for a given structure and select the structure which best agrees with the data.

4.2 Selecting a plausible structure which best agrees with the data

For a given triaxial shape (with semi-axial dimensions a > b > c) *P* (and hence f/f_o, $s^o_{20,w}$) together with a comprehensive set of other hydrodynamic shape functions can be evaluated using the routine *ELLIPS2* (32). The sedimentation and other hydrodynamic properties of different structures of different axial ratios (a/b, b/c) can then be compared directly. To assist this, the (a/b, b/c) ratios from a crystal structure can be first evaluated using ellipsoid fitting to crystal co-ordinates using the routine *ELLIPSE* (37).

Many structures however cannot be represented by ellipsoidal shapes—even general triaxial ellipsoids. The classical example is the antibody molecule. For arbitrary-shaped particles, the structure is represented by a number of spherical beads. From user specified co-ordinates the hydrodynamic properties for the composite structure can be calculated: the most advanced routine for doing this is currently *SOLPRO* (33, 38, 39). Unlike those for ellipsoids the hydrodynamic relations for bead constructs are not exact, but they are generally a good approximation. In practice, modelling the surface as a structure with an array of beads (called 'bead-shell' or just 'shell' modelling) appears to be the most successful, although 'filling models' where both the surface and interior structure are represented by a series of small beads can give results seriously in error:

unfortunately this means that approaches that have been presented based on representing the complete set of atoms from a crystal structure with corresponding beads should be avoided. The potential user is recommended to consult a recent work by Carrasco (40).

5 Sedimentation velocity studies of ligand binding

Having completed the general treatment of the sedimentation velocity variant of analytical ultracentrifugation for the study of equilibria, we now turn to the specific problem of quantifying an acceptor–ligand interaction by sedimentation velocity. In that regard there are two situations that can be practically considered: that in which the acceptor is macromolecular (or particulate) and the ligand is small; and that in which both reactants are macromolecular.

5.1 Interactions of a (protein) acceptor with a small ligand

Provided that the binding of ligand is without effect on the sedimentation coefficient of the acceptor ($s_{ABi} = s_A$), the free concentration of ligand in an acceptor–ligand mixture is readily determined by sedimentation velocity. In the illustrative application of *Figure 5b*, the absorption optical system has been used to monitor the sedimentation velocity behaviour of a mixture of methyl orange (B) and bovine serum albumin (A) (41). At the speed of the experiment (59 780 r.p.m.) acceptor and acceptor–ligand complexes co-migrate with the sedimentation coefficient of albumin (4.4S) but there is effectively no sedimentation of methyl orange ($s_B = 0.2S$). Consequently, the sedimentation velocity pattern reflecting the ligand constituent is biphasic, with a sedimenting boundary separating the plateau of original composition (α-phase) from a region comprising pure methyl orange (β-phase). The co-migration of A and all AB_i complexes ensures the absence of any redistribution of methyl orange as the result of migration of the acceptor constituent; and hence allows C_B^β to be identified with C_B^α, the free *molar concentration* of ligand in the mixture if the 'rectangular approximation' is made (42, 43). As noted by Steinberg and Schachman (41), this conclusion requires slight modification in sedimentation velocity because of non-compliance with assumed migration in a rectangular cell under the influence of a homogeneous field. Sedimentation in a sector-shaped cell leads to radial dilution that decreases slightly the values of C_B^β, C_B^α, $\bar{C}_B^\alpha$, and $\bar{C}_A^\alpha$ from those that would have applied to a mixture with the loaded composition. However, in view of the uncertainty surrounding the assumed identity of sedimentation coefficients for acceptor and all acceptor–ligand complexes, results are usually interpreted on the basis of the identification of C_B^β with the free ligand concentration in a mixture with the composition that was subjected to sedimentation velocity. Inasmuch as the sole objective of the ultracentrifugation is to generate an acceptor-free region for measurement of the ligand concentration, the experiments may also be performed in a preparative centrifuge (44–48).

In situations where B is a small ligand such as a metal ion or a coenzyme, the

estimate of C_B^α is combined with the values of $\bar{C}_A^\alpha$ and $\bar{C}_B^\alpha$ to generate the binding function v:

$$v = (\bar{C}_B^\alpha - C_B^\alpha)/\bar{C}_A^\alpha \qquad [20]$$

the dependence of which upon C_B^α is interpreted in terms of the conventional binding equation:

$$v = pk_{AB}C_B^\alpha/(1 + k_{AB}C_B^\alpha) \qquad [21]$$

where k_{AB} denotes the intrinsic binding constant for the interaction with p equivalent and independent sites on the acceptor (49).

5.2 Interactions of an acceptor with a macromolecular ligand

For the interaction between an acceptor and a macromolecular ligand the sedimentation coefficient of the complex is likely to be greater than that of either reactant. Under those circumstances ($s_{AB} > s_A > s_B$ for a system with 1:1 complex formation) a reaction boundary and a boundary corresponding to a pure reactant are generated in a sedimentation velocity experiment (42, 50)—a feature illustrated in *Figure 6* for the electrostatic interaction between ovalbumin (A) and lysozyme (B) at neutral pH and low ionic strength (43). Schlieren patterns for the individual reactants are presented in Figures 6a and 6b, whereas *Figure 6c* refers to a mixture of lysozyme and ovalbumin in 1.5:1 molar ratio. A reaction boundary ($s = 4.2S$) and a lysozyme boundary ($s = 2.3S$) are clearly evident. However, only a single boundary is observed for a mixture with ovalbumin in molar excess (*Figure 6d*)—a reflection of incomplete resolution between a pure reactant phase (now ovalbumin) and the reaction boundary.

Even in situations where the sedimentation velocity pattern reflecting an acceptor–ligand interaction exhibits resolution of a pure reactant boundary (as in *Figure 6c*), the important point to note is that the ligand concentration in the pure-solute phase (say C_B^β) does not equal its concentration (C_B^α) in the
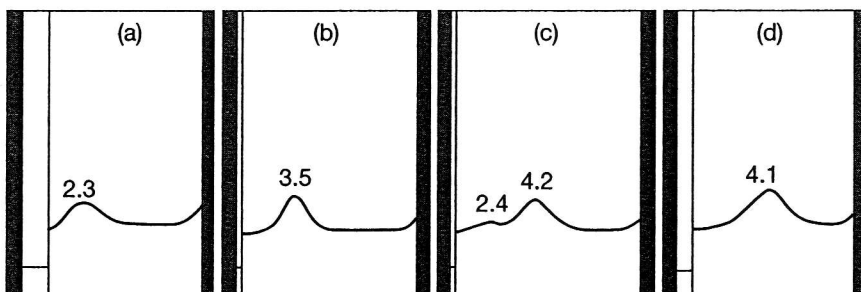
Figure 6 Schlieren patterns obtained in a study of the interaction between ovalbumin and lysozyme, pH 6.8, $I = 0.02$, by sedimentation velocity (59 780 r.p.m., 20 °C). (a) Lysozyme (0.28 mM). (b) Ovalbumin (0.14 mM). (c) Mixture of lysozyme (0.21 mM) and ovalbumin (0.13 mM). (d) Mixture of lysozyme (0.14 mM) and ovalbumin (0.16 mM). Data are taken from ref. 43.

equilibrium mixture for a system with $s_{AB} > s_A > s_B$. However, considerations of mass conservation (50–52) show that the free concentration of the other reactant, $C_A{}^\alpha$, may be determined from the expression:

$$C_A{}^\alpha = [\bar{C}_A{}^\alpha (\bar{s}_A - s_B) - \bar{C}_B{}^\alpha (s' - s_B) + C_B{}^\beta (s' - s_B)]/(\bar{s}_A - s_B) \qquad [22]$$

where $\bar{s}_A$, the average sedimentation coefficient of acceptor constituent, and s', the sedimentation coefficient of the boundary of ligand constituent within the reaction boundary, must both be taken as $s^{\alpha\beta}$, the sedimentation coefficient of the reaction boundary. A value of 3×10^4 M^{-1} for K_{AB} is obtained (43) by combining the value of $C_A{}^\alpha$ emanating from the application of *Equation 22* to the results from *Figure 6c* with the expression for the association equilibrium constant, namely:

$$K_{AB} = C_{AB}{}^\alpha/(C_A{}^\alpha C_B{}^\alpha) = (\bar{C}_A{}^\alpha - C_A{}^\alpha)/[C_A{}^\alpha (\bar{C}_B{}^\alpha - \bar{C}_A{}^\alpha + C_A{}^\alpha)] \qquad [23]$$

In keeping with sedimentation velocity studies of acceptor interactions with small ligands, the 'rectangular approximation' is inherent in *Equation 22*, as is neglect of the composition dependence of the sedimentation coefficients of individual species (s_A, s_B). These problems also pervade the characterization of acceptor–ligand interactions by an alternative sedimentation velocity procedure —interpretation of the constituent sedimentation coefficients $\bar{s}_A$ and $\bar{s}_B$.

Inasmuch as the constituent sedimentation coefficients of the two solute components in an acceptor–ligand system undergoing 1:1 complex formation are given by:

$$\bar{s}_A = (s_A C_A{}^\alpha + s_{AB} C_{AB}{}^\alpha)/\bar{C}_A{}^\alpha \qquad [24a]$$

$$\bar{s}_B = (s_B C_B{}^\alpha + s_{AB} C_{AB}{}^\alpha)/\bar{C}_B{}^\alpha \qquad [24b]$$

it follows that $\bar{s}_A$ is a function of mixture composition provided that acceptor-ligand complex migrates faster than A ($s_{AB} > s_A$). For the ligand constituent the corresponding proviso that $s_{AB} > s_B$ always pertains, and hence $\bar{s}_B$ invariably shows a progressive increase for mixtures with increasing constituent concentration of one reactant but fixed constituent concentration of the other. Elimination of $C_{AB}{}^\alpha$ from Equations 24a and 24b on the grounds that $C_{AB}{}^\alpha = (\bar{C}_A{}^\alpha - C_A{}^\alpha)$ $= (\bar{C}_B{}^\alpha - C_B{}^\alpha)$ for an interaction confined to 1:1 stoichiometry leads to the following expressions for the concentration of free reactant.

$$C_A{}^\alpha = \bar{C}_A{}^\alpha (s_{AB} - \bar{s}_A)/(s_{AB} - s_A) \qquad [25a]$$

$$C_B{}^\alpha = \bar{C}_B{}^\alpha (s_{AB} - \bar{s}_B)/(s_{AB} - s_B) \qquad [25b]$$

The value of s_i (where i = A or B) may be determined by application of the basic transport equation:

$$\bar{s}_i = -(1/2\omega^2 t) \ln [\{2 \int_{r_a}^{r_p} r \, \bar{C}_i(r) \, dr\}/ (r_p{}^2 \bar{C}_i{}^\circ) + (r_a{}^2/r_p{}^2)] \qquad [26]$$

to a sedimentation velocity distribution recorded at effective time t after attainment of angular velocity ω (40). In *Equation 26* the integration covers radial distances from the air–liquid meniscus r_a to a position r_p in the α-plateau region beyond the $\alpha\beta$ reaction boundary; and $\bar{C}_i{}^\circ$ denotes the total concentration of
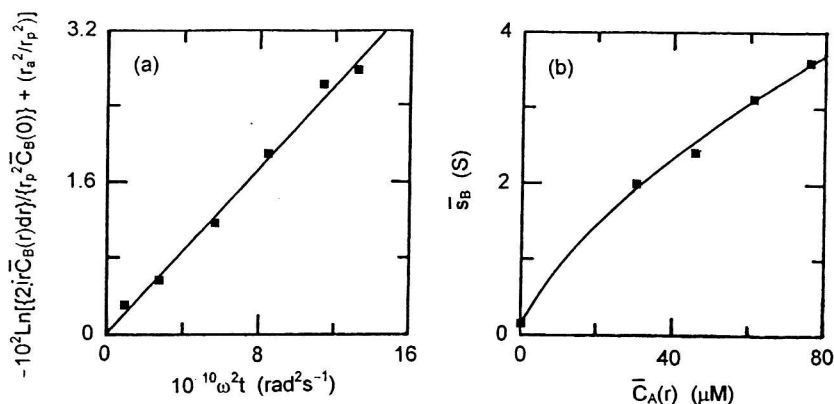
Figure 7 Use of constituent sedimentation coefficients for the characterization of an acceptor–ligand interaction. (a) Determination of $\bar{s}_B$ by the application of *Equation 7* to distributions for the ligand constituent obtained by subjecting a mixture of methyl orange (30 μM) and bovine serum albumin (45 μM) to sedimentation at 59 780 r.p.m. and 20 °C for the indicated times in a Beckman model E ultracentrifuge. (b) Dependence of $\bar{s}_B$ upon albumin concentrations in mixtures with a fixed concentration (30 μM) of methyl orange. Data are taken from ref. 41.

component i in the loaded mixture. For the application of this expression $\bar{C}_i^{\,o}$ and $\bar{C}_i(r)$ may be replaced by the corresponding optical parameters (e.g. absorbance); and the product $\omega^2 t$ is recorded as part of the printout for each recorded distribution in the XL-A and XL-I ultracentrifuges.

The measurement of $\bar{s}_B$ by means of *Equation 26* is illustrated in *Figure 7a*, which refers to a sedimentation velocity experiment conducted at 58 780 r.p.m. on a mixture of bovine serum albumin (45 μM) and methyl orange (30 μM): a value of 2.4S for $\bar{s}_B$ is obtained from the slope (41). Although the values of $\bar{s}_B$ obtained with the same methyl orange concentration and a range of albumin concentrations exhibit the predicted increase with increasing $\bar{C}_A^{\,\alpha}$ (*Figure 7b*), their quantitative interpretation by the above procedure is precluded by nonconformity with the assumed 1:1 stoichiometry of the acceptor–ligand interaction.

5.3 Sedimentation velocity studies of weak interactions

For weak interactions the negative dependence of sedimentation coefficient upon solute concentration needs to be taken into account. To that end a procedure called *SA-PLOT* has been developed around the general concentration dependence expressions (Equations 15 and 16) to allow simulation of a dependence of $\bar{s}$ (the weight-average sedimentation coefficient) upon total solute concentration that can be compared with its experimental counterpart. This procedure is designed primarily for the characterization of solute self-association, but can also be used for studies of the interaction between reactants with identical sedimentation coefficients. For a monomer–dimer system the statement of mass conservation:

$$\bar{c} = c_1 + 2c_1^{\,2}/(K_d M_1) \tag{27}$$

94

is a quadratic equation with solution:

$$c_1 = K_dM_1[-1 + \{1 + 8\bar{c}/(K_dM_1)\}^{1/2}]/4 \tag{28}$$

which allows the monomer concentration, c_1, and dimer concentration, $c_2 = \bar{c} - c_1$, to be calculated for any specified magnitude of the dissociation constant K_d. Combination of these values of c_1 and c_2 with the magnitudes of the corresponding sedimentation coefficients (s_1 and s_2) calculated from *Equations 15* and *16* on the basis that $\bar{c}$ is the appropriate concentration then allows estimation of the dependence of $\bar{s}$ (*Equation 24*) upon $\bar{c}$. The program *SA-PLOT* utilizes Equations 15, 16, 24, and 28 to compute $\bar{s}$ as a function of $\bar{c}$ for an assigned value of the dissociation constant, which is then refined iteratively on the basis of minimizing the sums of squares of residuals between experimental data and the simulated dependencies for designated K_d values. As noted above, the *SA-PLOT* program can also to be applied to a 1:1 interaction between different proteins (53), provided that their molecular masses and hence sedimentation coefficients are within 10–15% of each other (*Figure 8*).

5.4 The shape of sedimenting boundaries for acceptor–ligand systems

Thus far we have presented characterizations of an acceptor–ligand interaction on the basis of the size of the reactant boundary (C_B^β) and the composition dependence of the magnitude of constituent sedimentation coefficients. Neither of these procedures has taken advantage of the detailed form of the sedimenting boundary system, which is undoubtedly the most striking aspect of a
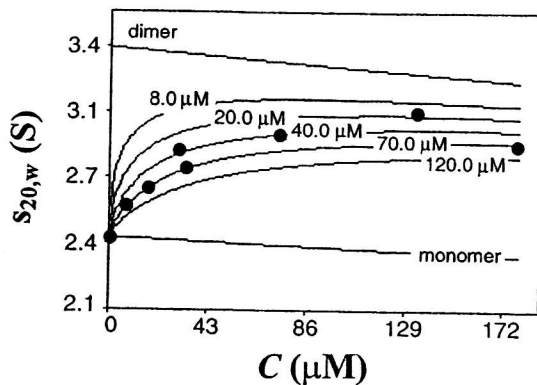

Figure 8 Concentration dependence of the sedimentation coefficient for a protein interacting with a macromolecular ligand (another protein): the cell adhesion molecule CD42 with its counter-receptor CD48. The two have similar molecular weights ($\sim$ 28 500) and the interaction can be regarded as an effective 'monomer–dimer' system. Concentration expressed in molar terms (with respect to monomer). The (weight average) sedimentation coefficient data points ($\bullet$) are modelled iteratively to Equations 15, 16, 24, and 28 {with k_s (monomer) set as 5 ml/g; k_s (dimer) as 8.5 ml/g} for values of the dissociation constant K_d in the ranges 8–120 μM using the software *SA-PLOT*. From ref. 53 and reproduced courtesy of Springer–Verlag.

sedimentation velocity distribution. These boundary forms are more distinctive when plotted in derivative format (dc/dr versus r)—the distribution recorded by the schlieren optical system that has been omitted from the current generation of analytical ultracentrifuges. However, a procedure has been devised (54–56) whereby the equivalent shape of the derivative distribution is extracted from the optically recorded integral distribution (concentration or absorbance as a function of radial distance).

Results from application of the $g(s^*)$ procedure to sedimentation velocity distributions for an acceptor-ligand system are presented in *Figure 9*, which refers to the interaction between diphtheria toxin and an elicited monoclonal antibody (56). Studies at neutral pH were used to establish the forms of the normalized derivative distributions, $g(s^*)$ versus s^*, for the toxin (B) alone, the antibody (A), and the AB_2 complex (*Figure 9a*). Adjustment of a solution of AB_2 complex to pH 5 causes the complex to undergo dissociation in a manner such that the distribution remains essentially unimodal despite the coexistence of species with molecular masses of 266, 150, and 58 kDa (*Figure 9b*). Such behaviour is typical of a system in rapid association equilibrium, for which the major indicator of dissociation is the observation that dilution leads to a progressive decrease in the value of s^* at the peak of the distribution. Clearly, there is far more potential information to be gained from the shapes of these patterns than simply the value of a constituent sedimentation coefficient, $\bar{s}$ (or $\bar{s}^*$).

What is really required is an analytical solution to the differential equation describing mass migration in a sedimentation velocity experiment—the Lamm equation—which for a single non-interacting solute is given by *Equation 8*. However, that problem is seemingly intractable. Our understanding of the shapes of sedimentation velocity patterns has therefore stemmed from the pioneering studies of Gilbert (42, 57), who established the forms of such distributions by obtaining analytical solutions to the differential equations describing diffusion-
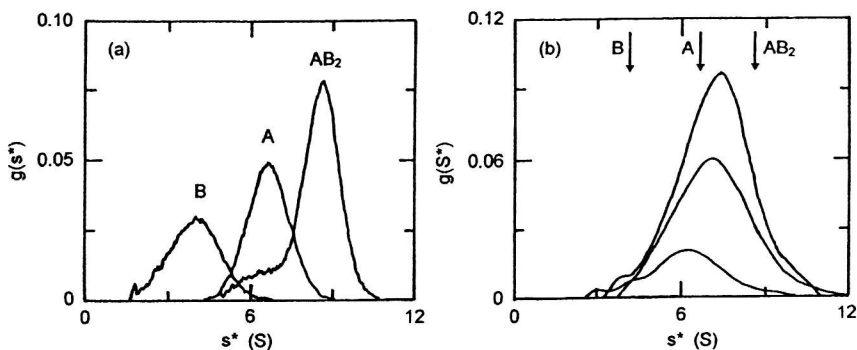

Figure 9 Use of the $g(s^*)$ analysis (13) to deduce the equivalent of schlieren patterns from integral sedimentation velocity distributions for a system comprising the interaction of diphtheria toxin (B) with biospecific monoclonal antibody (A). (a) $g(s^*)$-s^* distributions for the two separate reactants and for the stable AB_2 complex at neutral pH. (b) Corresponding patterns deduced from integral distributions for the indicated concentrations of complex at pH 5.0. Data are taken from ref. 56.

free migration. Despite the passage of nearly four decades, those publications and another that tackled the same problem in a different manner (50, 58) are pivotal to our understanding of the effects of chemical re-equilibration in sedimentation velocity experiments. Indeed, use has already been made of those findings to characterize systems with $s_{AB} = s_A > s_B$ (*Figure 6*) and $s_{AB} > s_A > s_B$ (*Figure 9*).

From the viewpoint of comparing experimental patterns with such predicted behaviour, the absence of diffusional effects in the latter has been a large impediment to the exercise. *Figures 10a* and *10b* depict the theoretical diffusion-free behaviour that led to the interpretation of sedimentation velocity patterns for the ovalbumin–lysozyme system (*Figures 6c* and *6d*). In that regard the failure to observe an ovalbumin (A) boundary (*Figure 6d*) under conditions comparable with those pertaining in *Figure 11b* has been explained on the grounds that diffusional spreading would have disguised the predicted resolution. Although such rationalization is certainly reasonable, the inference would obviously benefit from the generation of a predicted distribution that also takes into account the effects of diffusional spreading.

Boundary spreading due to the effects of diffusion is now usually incorporated into theoretical sedimentation velocity distributions by solving numerically the Lamm equation by the finite element treatment of Claverie (59–61). To date the major use of this approach has been to accommodate the effects of concentration-
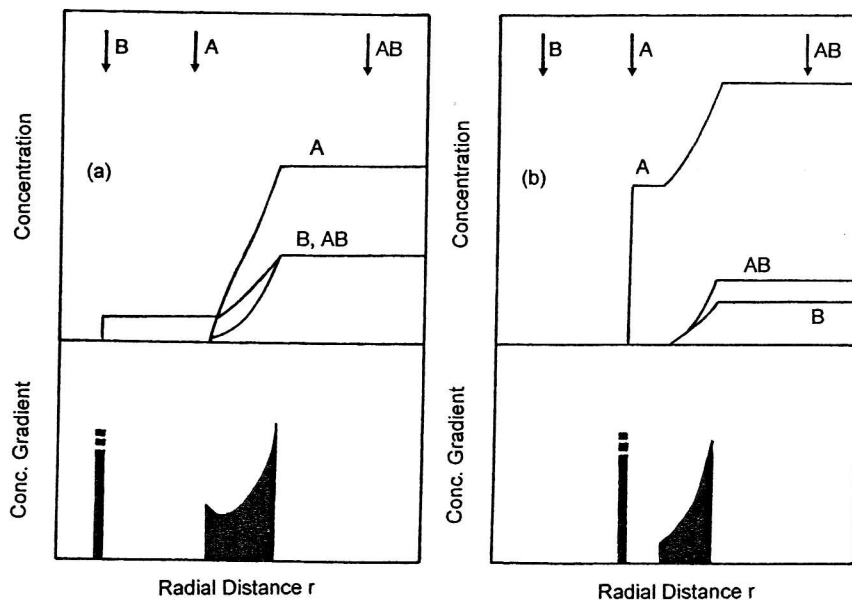
Figure 10 Illustrative diffusion-free sedimentation velocity patterns for acceptor–ligand interactions with $s_{AB} > s_A > s_B$. (a) Sedimentation velocity distributions for a mixture of acceptor and ligand with ligand (B) in molar excess. (b) Corresponding distribution for a mixture with acceptor (A) in molar excess. In each case the upper pattern is the integral whereas the lower represents the derivative (schlieren) pattern. Details of the manner in which such patterns are deduced are to be found in refs 42, 50, and 57.

dependence of s and D for a single, non-interacting solute on migration and boundary spreading. Use of the Claverie method to obtain the best-fit description of the migration and boundary spreading in terms of *Equation 4* and the corresponding equation for the translational diffusion coefficient:

$$(D_A)_{20,w} = (D_A^\circ)_{20,w}(1 + k_D c + ..)\qquad [29]$$

leads to unique identification of the molar mass by combining the estimates of $(s_A^\circ)_{20,w}$ and $(D_A^\circ)_{20,w}$ (62–65).

Application of the technique to a system undergoing chemical re-equilibration entails alternating rounds of simulated transport and chemical reaction—the procedure introduced by Cann and Goad (66) to modify the values of the sedimentation and diffusion coefficients (now s_i and D_i) for solution of the Lamm equation by the finite difference method. Details of the finite element and finite difference approaches are reviewed by Cox and Dale (67), who discuss the potential of the Claverie method for simulating the sedimentation velocity behaviour of chemically reacting systems involving solute self-association as well as interactions between dissimilar reactants. This approach is now being actively pursued in the realm of solute self-association (62, 63) and also interactions between two solute components (68, 69).

Despite its sophistication and ability to generate sedimentation velocity patterns with a greater sense of experimental realism, this numerical solution of the Lamm equation is not necessarily providing an accurate description of the sedimentation behaviour of an interacting system. A major limitation is likely to be inadequacy of the expressions (the counterparts of *Equations 4* and *29*) invoked to describe the composition dependence of s and D for the individual species. In that regard the necessity to assign magnitudes to sedimentation coefficients (s_i°) for any postulated complex species AB_i has already been addressed in discussing the use of constituent sedimentation coefficients for characterizing interactions. There is also a problem with specifying the forms of the composition dependence of s and D arising from non-chemical interactions between species, there being no theoretical justification for the commonly used substitution of total solute concentration $\bar{c}$ for c in *Equations 4* and *29*. Furthermore, in view of the number of parameters requiring evaluation by curve-fitting, the method is unlikely to become a major contender for deducing the stoichiometry and strength of acceptor-ligand interactions. Nevertheless, it has considerable potential for testing further the adequacy of a quantitative description of an acceptor–ligand interaction that has been obtained by other means.

6 The study of ligand-mediated conformational changes

Elucidation of the mechanism responsible for the allosteric behaviour of enzymes has inevitably posed a problem because of the need to distinguish between models based on pre-existence (70) and ligand-induction (71) of the enzyme isomerization. Sedimentation velocity provides a powerful means of detecting

the change in enzyme shape; and, in favourable circumstances, the means of distinguishing between pre-existing and ligand-induced isomerization of the acceptor.
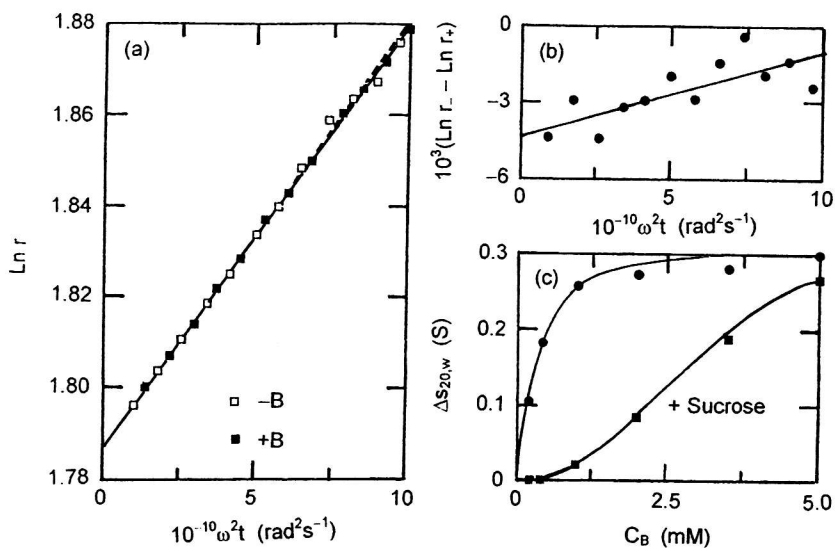
Difference sedimentation velocity (72, 73) was introduced over 30 years ago as a means of quantifying ligand-mediated conformational changes in enzymes in terms of differences in hydrodynamic volume (74). Such changes were quantified initially on the basis of the difference between values of the sedimentation coefficients obtained from simultaneous velocity runs on enzyme solutions with and without ligand. However, more recent studies (75–77) have employed the expression (75):

$$d(\ln r_- - \ln r_+)/dt = \omega^2(s_- - s_+) \qquad [30]$$

where r_- and r_+ are the respective radial positions of the boundaries in the ligand-free and ligand-containing solutions after centrifugation at angular velocity ω for time t. Provided that the optical records for both solutions are recorded simultaneously, the difference in sedimentation coefficients is obtained from the slope of the dependence of $(\ln r_- - \ln r_+)$ upon t.

Because the design of the Beckman XL-A and XL-I ultracentrifuges precludes the simultaneous recording of solute distributions in two cells, the two distributions being compared must be recorded sequentially. Provided that the time increment between the recording of the distributions in the two cells is constant, *Equation 30* with t taken as the time for the first of the paired distributions, continues to provide an exact description of the difference in sedimentation coefficients. Although the fluctuation of the time increment by 3–4% about a mean in the XL-A ultracentrifuge is at variance with this proviso, the random error associated with boundary location is likely to render insignificant the relatively minor departure from the predictions of *Equation 28*; and accordingly difference sedimentation velocity studies can be pursued with confidence in the current (as well as older) generation of analytical ultracentrifuges (78). We illustrate the potential of difference sedimentation velocity for the detection and quantification of the small changes in sedimentation coefficient of rabbit muscle pyruvate kinase in the presence of phenylalanine, an allosteric inhibitor of the enzyme.

Determination of sedimentation coefficients from the two separate time dependencies of the logarithm of radial distance migrated is presented in *Figure 11a*, which signifies a slightly faster migration rate for enzyme alone than for enzyme in the presence of a saturating concentration (5 mM) of phenylalanine. Although the independent estimates of 9.5 ($\pm$ 0.3) and 9.2 ($\pm$ 0.2)S for pyruvate kinase in the absence and presence of phenylalanine indicate a probable difference of 0.3S between the sedimentation coefficients of enzyme and enzyme–inhibitor complex, the result, 0.3 ($\pm$ 0.5)S is clearly equivocal. On the other hand, the difference plot of results according to *Equation 30* is far more definitive in that regard (*Figure 11b*) inasmuch as linear regression analysis yields a slope, $\Delta s = (s_- - s_+)$, of 0.31 ($\pm$ 0.08)S (78). Earlier results (77) for the dependence of the sedimentation coefficient difference upon phenylalanine concentration are

Figure 11 Studies of ligand-mediated conformational changes in rabbit muscle pyruvate kinase (pH 7.5, I = 0.13) by difference sedimentation velocity. (a) Separate measurement of the sedimentation coefficients of enzyme alone and in the presence of phenylalanine (5 mM). (b) Direct comparison of the two sedimentation coefficients by difference sedimentation velocity, the results being plotted according to *Equation 30*. (c) Dependence of the difference in sedimentation coefficient upon phenylalanine concentration, together with the effect of molecular crowding by sucrose (0.1 M) on that difference. Data in (a) and (b) are taken from ref. 78, and those in (c) from ref. 77.

summarized (●) in *Figure 11c*. A corresponding comparison of sedimentation co-efficients for pyruvate kinase in the absence and presence of phosho*enol*pyruvate (1 mM) yielded a value of −0.03 (± 0.01)S for Δs, which signifies the likelihood that the sedimentation coefficient of 9.5S for enzyme alone is the weight-average for an equilibrium mixture of species with sedimentation coefficients of 9.47 and 9.81S. In that regard the consequent isomerization constant of 0.09 so determined matches the value deduced (79) by analysis of enzyme kinetic data in terms of the Monod model.

The question of the pre-existence or ligand-induction of the conformational change in the enzyme giving rise to the sedimentation coefficient difference can be addressed further by taking advantage of thermodynamic non-ideality arising from the crowding effect of a high concentration of an inert co-solute. Entropic considerations dictate that a crowded environment should displace any enzyme isomeric equilibrium in favour of the smaller isomer—a phenomenon illustrated in *Figure 11c* by the diminished magnitudes of Δs observed in the presence of 0.1 M sucrose (■).

To test whether the difference sedimentation velocity result obtained with phospho*enol*pyruvate reflected perturbation of a pre-existing isomerization in favour of the smaller enzyme state, the experiment was repeated in buffer sup-plemented with 0.1 M sucrose (77). The lack of an effect of phosph*enol*pyruvate

on this occasion, $\Delta s_{20,w} = -0.003 (\pm 0.005)S$, indicates that a high concentration of inert co-solute can also bring about the change in sedimentation coefficient effected by substrate. Such displacement of an isomerization equilibrium in the absence of substrate (ligand) establishes its pre-existence; and hence justifies consideration of the rabbit muscle pyruvate kinase system in terms of the Monod model of allostery.

This experimental illustration of the use of an inert co-solute for detecting protein isomerizations demonstrates the potential of thermodynamic non-ideality as a means of probing such phenomena. Indeed, the above combination of difference sedimentation velocity and molecular crowding effects has been used subsequently to establish that the conformational change undergone by yeast hexokinase as the result of glucose binding also reflects preferential interaction of substrate with an equilibrium mixture of isomeric enzyme states (78). Determining the nature of an isomerization (pre-existing or ligand-induced) had previously been a seemingly intractable problem to which there was no unequivocal solution: but now there is one.

7 Concluding remarks

Sedimentation velocity is frequently the method by which a reversible macro-molecular interaction is detected during routine monitoring of the purification and properties of a protein or enzyme. The existence of solute self-association or reversible interaction between dissimilar reactants gives rise to distinctive sedimentation velocity behaviour, which may be used not only as a diagnostic of species interconversion but also as a means of obtaining a preliminary characterization of the interaction. Indeed, sedimentation velocity has proven the method of choice for examining the effects of small ligands on the inter-conversion between the two isomeric states of allosteric enzymes.

Absolute characterization of the equilibrium constant and reaction stoichiometry for an interaction involving a change in molecular mass is precluded by the dependence of the sedimentation coefficient upon the shape as well as size of the resulting complex species—a situation that necessitates resort to a model of any putative complex species in order to specify the magnitude of its sedimentation coefficient. However, the preliminary characterization afforded by the analysis of sedimentation velocity behaviour can be used to advantage in the design of subsequent sedimentation equilibrium studies. The latter have the potential to afford a more definitive characterization of the interaction because the molecular mass of any postulated complex species may be assigned unequivocally from those of the reactants and the specified stoichiometry. Such characterization of macromolecular interactions by sedimentation equilibrium is discussed in the next chapter.

References

1. Gerhart, J. C. and Schachman, H. K. (1968). *Biochemistry*, **7**, 538.
2. Harris, S. J. and Winzor, D. J. (1988). *Arch. Biochem. Biophys.*, **265**, 458.

3. Fujita, H. (1956). *J. Chem. Phys.*, **24**, 1084.

4. Baldwin, R. L. (1957). *Biochem. J.*, **65**, 503.

5. Creeth, J. M. and Winzor, D. J. (1962). *Biochem. J.*, **83**, 566.

6. Van Holde, K. E. (1960). *J. Phys. Chem.*, **64**, 1582.

7 Inkerman, P. A., Winzor, D. J., and Zerner, B. (1975). *Can. J. Biochem.*, **53**, 547.

8. Claverie, J.-M., Dreux, H., and Cohen, R. (1975). *Biopolymers*, **14**, 1685.

9. Cohen, R. and Claverie, J.-M. (1975). *Biopolymers*, **14**, 1701.

10. Claverie, J.-M. (1976). *Biopolymers*, **15**, 843.

11. Behlke, J. and Ristau, O. (1997). *Biophys. J.*, **72**, 428.

12. Demeler, B. and Shaker, H. (1997). *Biophys. J.*, **74**, 444.

13. Schuck, P. and Millar, D. B. (1998). *Anal. Biochem.*, **259**, 48.

14. Schuck, P. (1998). *Biophys. J.*, **75**, 1503.

15. See the Web site: http://www.nottingham.ac.uk/ncmh/ and Helmut Coelfen<coelfen@mpikg-teltow.mpg.de>

16. Philo, J. (1994). *Biophys. J.* **72**, 435.

17. Lamm, O. (1929). *Z. Physik. Chem. (Leipzig)*, **A143**, 177.

18. Stafford, W. F. (1992). *Anal. Biochem.*, **203**, 295.

19. Van Holde, K. E. and Weischet, W. O. (1978). *Biopolymers*, **17**, 1387. See also the Web site: http://www.biochem.uthscsa.edu/UltraScan

20. See the Web site: ftp://alpha.bbri.org/rasmb/spin/ms_dos/sednterp.

21. Kratky, O., Leopold, H., and Stabinger, H. (1973). In *Methods in Enzymology*, Vol. 27, p. 98.

22. Schachman, H. K. (1959). *Ultracentrifugation in biochemistry*. Academic Press, New York.

23. Lloyd, P. H. (1974). *Optical methods in ultracentrifugation, electrophoresis and diffusion with a guide to the interpretation of optical records*. Oxford Univ. Press, Fairlawn, NJ.

24. Johann, C., Thiessen, A., Deacon, M. P. and Harding, S. E. (1999). *Refractive increment data book*. Nottingham Univ. Press, Nottingham, UK.

25. See Ertughrul, O. W. D., Errington, N., Raza, S., Sutcliffe, M. J., Rowe, A. J., and Scrutton, N. S. (19XX). *Protein Eng.*, **11**, 447

26. Cherwell Scientific Limited, Oxford; UK.

27. Johnston, J. P. and Ogston, A. G. (1946). *Trans. Faraday Soc.*, **42**, 789.

28. Rowe, A. J., Wynne Jones, S., Thomas, D. G., and Harding, S. E. (1992). In *Analytical ultracentrifugation in biochemistry and polymer science* (ed. S. E. Harding, A. J. Rowe, and S. E. Horton), pp. 49–62. Royal Society of Chemistry, Cambridge, UK.

29. Harding, S. E. (1995). *Biophys. Chem.*, **55**, 69.

30. Harding, S. E., Davis, S. S., Deacon, M. P., and Fiebrig, I. (1998). *Biotechnol. Genet. Eng. Rev.*, **16**, 41.

31. Deacon, M. P., Davis, S. S., White, R. J., Nordman, H., Carlstedt, I., Errington, N., *et al.* (1999). *Carbohydr. Polym.*, **38**, 235.

32. Harding, S. E., Horton, J. C., and Colfen, H. (1997). *Eur. Biophys. J.*, **25**, 347.

33. Garcia de la Torre, J., Carrasco, B., and Harding, S. E. (1997). *Eur. Biophys. J.*, **25**, 361.

34. Pavlov, G. M., Rowe, A. J., and Harding, S. E. (1997). *Trends Anal. Chem.*, **16**, 401.

35. Gralén, N. (1944). PhD Dissertation, University of Uppsala.

36. Creeth, J. M. and Knight, C. G. (1965). *Biochim. Biophys. Acta*, **102**, 549.

37. Taylor, W. R., Thornton, J. M., and Turnell, R. J. (1980). *J. Mol. Graph.*, **1**, 30.

38. Garcia de la Torre, J., Harding, S. E., and Carrasco, B. (1999). *Eur. Biophys. J.*, **28**, 119.

39. Garcia de la Torre, J., Harding, S. E., and Carrasco, B. (1998). *Biochem. Soc. Trans.*, **26**, 716.

40. Carrasco, B. (1998). PhD Thesis, Universidad de Murcia.

41. Steinberg, I. Z. and Schachman, H. K. (1966). *Biochemistry*, **5**, 3728.

42. Gilbert, G. A. and Jenkins, R. C. L. (1959). *Proc. R. Soc. London, Ser. A*, **253**, 420.

43. Nichol, L. W. and Winzor, D. J. (1964). *J. Phys. Chem.*, **68**, 2455.

44. Chanutin, A., Ludewig, S., and Masket, A. V. (1942). *J. Biol. Chem.*, **143**, 737.

45. Velick, S. F., Hayes, J. E., Jr., and Harting, J. (1953). *J. Biol. Chem.*, **203**, 527.

46. Velick, S. F. and Hayes, J. E., Jr. (1953). *J. Biol. Chem.*, **203**, 545.

47. Arnold, H. and Pette, D. (1968). *Eur. J. Biochem.*, **6**, 163.

48. Clarke, F. M. and Masters, C. J. (1972). *Arch. Biochem. Biophys.*, **153**, 258.

49. Klotz, I. M. (1946). *Arch. Biochem.*, **9**, 109.

50. Nichol, L. W. and Ogston, A. G. (1965). *Proc. R. Soc. London, Ser. B*, **163**, 343.

51. Nichol, L. W. and Ogston, A. G. (1965). *J. Phys. Chem.*, **69**, 1754.

52. Longsworth, L. G. (1959). In *Electrophoresis, theory, methods, and applications* (ed. M. Bier), p. 91. Academic Press, New York.

53. Silkowski, H., Davis, S. J., Barclay, A. N., Rowe, A. J., Harding, S. E., and Byron, O. (1997). *Eur. Biophys. J.*, **25**, 455.

54. Stafford, W. F. (1992). *Anal. Biochem.*, **203**, 295.

55. Stafford, W. F. (1994). In *Methods in Enzymology*, Vol. 240, p. 478.

56. Raso, V., Brown, M., McGrath, J., Liu, S., and Stafford, W. F. (1997). *J. Biol. Chem.*, **272**, 27618.

57. Gilbert, G. A. (1959). *Proc. R. Soc. London, Ser. A*, **250**, 377.

58. Nichol, L. W. and Winzor, D. J. (1972). *Migration of interacting systems*. Clarendon Press, Oxford.

59. Claverie, J.-M., Dreux, H., and Cohen, R. (1975). *Biopolymers*, **14**, 1685.

60. Cohen, R. and Claverie, J.-M. (1975). *Biopolymers*, **14**, 1701.

61. Claverie, J.-M. (1976). *Biopolymers*, **15**, 843.

62. Behlke, J. and Ristau, O. (1997). *Biophys. J.*, **72**, 428.

63. Demeler, B. and Shaker, H. (1997). *Biophys. J.*, **74**, 444.

64. Schuck, P. and Millar, D. B. (1998). *Anal. Biochem.*, **259**, 48.

65. Schuck, P. (1998). *Biophys. J.*, **75**, 1503.

66. Cann, J. R. (1970). *Interacting macromolecules*. Academic Press, New York.

67. Cox, D. J. and Dale, R. S. (1981). In *Protein-protein interactions* (ed. C. Frieden and L. W. Nichol), p. 173. Wiley, New York.

68. Behlke, J., Ristau, O., and Schonfeld, H. J. (1997). *Biochemistry*, **36**, 5149.

69. Behlke, J. and Ristau, O. (1997). *Eur. Biophys. J.*, **25**, 325.

70. Monod, J., Wyman, J., and Changeux, J.-P. (1965). *J. Mol. Biol.*, **12**, 88.

71. Koshland, D. E., Jr., Némethy, G., and Filmer, D. (1966). *Biochemistry*, **5**, 365.

72. Gerhart, J. C. and Schachman, H. K. (1968). *Biochemistry*, **7**, 538.

73. Schumaker, V. N. and Adams, P. (1968). *Biochemistry*, **7**, 3422.

74. Schumaker, V. N. (1968). *Biochemistry*, **7**, 3427.

75. Howlett, G. J. and Schachman, H. K. (1977). *Biochemistry*, **16**, 5077.

76. Oberfelder, R. W., Barisas, B. G., and Lee, J. C. (1984). *Biochemistry*, **23**, 3822.

77. Harris, S. J. and Winzor, D. J. (1988). *Arch. Biochem. Biophys.*, **265**, 458.

78. Jacobsen, M. P. and Winzor, D. J. (1997). *Prog. Colloid Polym. Sci.*, **107**, 82.

79. Oberfelder, R. W., Lee, L. L.-Y., and Lee, J. C. (1984). *Biochemistry*, **23**, 3813.

80. Ralston, G. (1993). *Introduction to analytical ultracentrifugation*. Beckman Instruments Inc., Fullerton, California, USA.

81. Morgan, P. J., Harding, S. E., Plyte, S. E., and Kneale, G. G. (1989). *Biochem. Soc. Trans.*, **17**, 234.

82. Marsh, E. N. and Harding, S. E. (1993). *Biochem. J.*, **290**, 551.